Synthesis of a Spatially Band-Limited Plane Wave in the Time-Domain Using Wave Field Synthesis

Nara Hahn, Fiete Winter, and Sascha Spors

Institute of Communications Engineering, University of Rostock, Germany

Email: nara.hahn@uni-rostock.de

Abstract—Wave Field Synthesis (WFS) is a spatial sound reproduction technique aiming at a physically accurate reconstruction of a desired sound field within an extended listening area. It was shown in a recent study that the accuracy of the synthesized sound field can be improved in a local area by applying a spatial band-limitation to the driving function. However, the computational complexity of the frequency-domain driving function is demanding because of the involved Bessel functions. In this paper, a time-domain WFS driving function is introduced for the synthesis of a spatially band-limited plane wave. The driving function is obtained based on a time-domain representation of the sound field which is given as a superposition of plane waves with time-varying direction and amplitude. The performance of the proposed approach is evaluated by numerical simulations. Practical issues regarding the discretization of the analytic driving function and dynamic range control are discussed.

I. INTRODUCTION

Wave Field Synthesis (WFS) and Near-field Compensated Higher-order Ambisonics (NFC-HOA) are two well known sound field synthesis techniques developed for a physically accurate reconstruction of a desired sound field using a loudspeaker array [1]–[5]. The loudspeakers, termed secondary sources, are driven in such a way that the superposition of the individual sound fields matches the desired field. One of the main difference between WFS and NFC-HOA is the mathematical representation of the desired sound field, from which the driving function is derived. In NFC-HOA, the sound field as well as the driving function are given as a spherical/circular harmonics expansion with respect to the center of the spherical/circular secondary source distribution. In a practical system, only a finite number of secondary sources are available which constitutes a discretization of the secondary source distribution leading to spectral repetitions in the harmonics domain [6]. To avoid spectral overlap, i.e. spatial aliasing, the harmonics expansion is truncated to a finite order [7, Sec. 4.4.1]. Typical NFC-HOA driving functions thus have finite spatial bandwidth, whereas conventional WFS driving functions exhibit infinite spatial bandwidth [8].

While such a spatial band-limitation causes deviations in representing a sound field, there are also benefits that can be exploited. As observed in a number of studies [4], [9], the synthesized sound field of NFC-HOA exhibits high accuracy at the center of expansion. This comes at the cost of impaired physical and perceptual qualities at off-center positions [8]–[10]. Therefore, NFC-HOA can be considered as a sound field synthesis technique aiming at an accurate synthesis within a local region, called local sound field synthesis. The location of the local listening area can be moved by re-expanding the sound field with respect to the center of the respective local listening area [11], [12].

The same principle can be applied to WFS. In [13], the WFS driving functions were derived based on an order-limited circular/spherical harmonics expansion of the desired sound field. As expected, an improved performance was achieved in the region centered around the expansion point. However, the driving functions introduced in [13, Table. 1] are available only in the time-frequency domain, and their implementation is computationally demanding as it requires the computation of Bessel and spherical Bessel functions.

In this paper, a time-domain driving function is proposed for the synthesis of a Dirac-shaped plane wave that exhibits a limited spatial bandwidth. The driving function is derived based on an analytic time-domain representation of the sound field (Sec. II). Two different derivations are introduced both of which lead to the same result. One is based on a circular harmonics expansion while the other on a plane wave decomposition. The proposed WFS driving function (Sec. III) is able to synthesize the sound field of a plane wave with a significantly reduced computational complexity. The spatio-temporal structure and the spectral responses of the synthesized sound fields are investigated by numerical simulations (Sec. V).

Nomenclature A position vector is denoted by lowercase boldface $\mathbf{x}$. The angular frequency is denoted by $\omega = 2\pi f$ with f being the temporal frequency. The speed of sound is denoted by c and the imaginary unit by i. Plane waves are assumed to propagate parallel to the xy-plane. The propagation direction is characterized by a normal vector $\mathbf{n}_{\text{pw}} = \big(\cos \phi_{\text{pw}}, \sin \phi_{\text{pw}}, 0 \big)$ where ϕ_{pw} denotes the azimuth angle.

II. TIME-DOMAIN REPRESENTATIONS OF A SPATIALLY BAND-LIMITED PLANE WAVE

A. Circular Harmonics Expansion

The sound field of a monochromatic plane wave $e^{-i\frac{\omega}{c} r \cos(\phi - \phi_{\text{pw}})}$ can be represented as a circular harmonics expansion for a given expansion center $\mathbf{x}_c$ [14, (2.44)]. By

truncating the order to $\pm M$, the infinite summation reduces to a finite series

$$S(\mathbf{x} - \mathbf{x}_c, \omega) =$$
$$= e^{-i\frac{\omega}{c}\langle \mathbf{n}_{\mathrm{pw}}, \mathbf{x}_c \rangle} \sum_{m=-M}^{M} i^{-m} J_m(\tfrac{\omega}{c} r') e^{im(\phi'-\phi_{\mathrm{pw}})}, \quad (1)$$

where $J_m(\cdot)$ denotes the Bessel function of order m. The inner product of two vectors is denoted by $\langle \cdot, \cdot \rangle$. Note that the truncated expansion is now an approximation of the plane wave with a limited accuracy [15]. The local coordinate system is defined as $\mathbf{x}' = \mathbf{x} - \mathbf{x}_c = (r'\cos\phi', r'\sin\phi', 0)$. Without loss of generality, $\mathbf{x}_c = \mathbf{0}$ is assumed in the remainder, thus $r' = r$ and $\phi' = \phi$.

The inverse Fourier transform of the Bessel function in (1) reads

$$\mathcal{F}^{-1}\{J_m(\tfrac{\omega}{c} r)\} = \frac{i^m}{\pi} \frac{\Pi\left(\frac{ct}{2r}\right) T_m\left(\frac{ct}{r}\right)}{\sqrt{(\frac{r}{c})^2 - t^2}}, \quad (2)$$

which can be obtained by reformulating Eq. (11.4.24) in [16]. $T_m(\cdot)$ denotes the Chebyshev polynomial of the first kind of degree m, and $\Pi\left(\frac{ct}{2r}\right)$ a rectangular function

$$\Pi(\tfrac{ct}{2r}) = \begin{cases} 1, & |t| < \frac{r}{c} \\ \frac{1}{2}, & |t| = \frac{r}{c} \\ 0, & \text{otherwise.} \end{cases} \quad (3)$$

The time-domain representation of (1) is thus obtained by replacing $J_m(\tfrac{\omega}{c} r)$ with (2),

$$s(\mathbf{x}, t)$$
$$= \frac{1}{\pi} \frac{\Pi\left(\frac{ct}{2r}\right)}{\sqrt{(\frac{r}{c})^2 - t^2}} \sum_{m=-M}^{M} T_m(\tfrac{ct}{r}) e^{im(\phi-\phi_{\mathrm{pw}})} \quad (4)$$

$$= \frac{1}{\pi} \frac{\Pi\left(\frac{ct}{2r}\right)}{\frac{r}{c}|\sin\beta(t)|} \sum_{m=-M}^{M} T_m(-\cos\beta(t)) e^{im(\phi-\phi_{\mathrm{pw}})}. \quad (5)$$

In the second equality, $-\frac{ct}{r}$ and $\sqrt{(\frac{r}{c})^2 - t^2}$ were replaced by $\cos\beta(t)$ and $|\sin\beta(t)|$, respectively. Equation (5) can be further simplified by exploiting $T_m(\cos\theta) = \cos(m\theta)$ [16, (22.3.15)] and the addition formula of cosine functions [16, (4.3.36) and (4.3.37)]

$$s(\mathbf{x}, t)$$
$$= \frac{1}{\pi} \frac{\Pi\left(\frac{ct}{2r}\right)}{\frac{r}{c}|\sin\beta(t)|} \sum_{m=-M}^{M} \cos\left(m(\beta(t)+\pi)\right) e^{im(\phi-\phi_{\mathrm{pw}})} \quad (6)$$

$$= \frac{1}{2\pi} \frac{\Pi\left(\frac{ct}{2r}\right)}{\frac{r}{c}|\sin\beta(t)|} \sum_{\mu\in\{\pm 1\}} \mathcal{D}_M\left(\phi - \phi_{\mathrm{pw}} + \pi + \mu\beta(t)\right), \quad (7)$$

where $\mathcal{D}_M(\theta) \equiv \sin\left(\frac{2M+1}{2}\theta\right)/\sin\left(\frac{\theta}{2}\right)$ denotes the periodic sinc function.

B. Plane Wave Decomposition

The time-domain representation can also be obtained from a plane wave decomposition

$$S(\mathbf{x}, \omega) = \frac{1}{2\pi} \int_0^{2\pi} \bar{S}(\alpha, \omega) e^{-i\frac{\omega}{c} r \cos(\phi-\alpha)} \mathrm{d}\alpha, \quad (8)$$
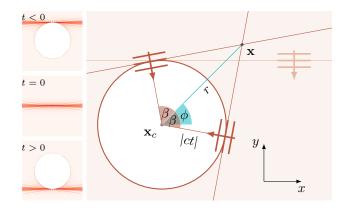

Fig. 1. Left: Simulated plane wave with a spatial bandwidth of $M = 29$. Snapshots for different time instances are shown in dB. Right: Illustration of a spatially band-limited plane wave for $-\frac{r}{c} < t < 0$. The original (Dirac-shaped) plane wave $\delta\left(t - \frac{r}{c}\cos(\phi - \phi_{\mathrm{pw}})\right)$ is indicated by ⚏. The expansion center is denoted by $\mathbf{x}_c$. The sound field consists of an infinite number of plane waves, forming a circular wavefront with radius $|ct|$. Two instantaneous plane waves ⚏ passing $\mathbf{x}$ propagate with angles of $\phi + \pi \pm \beta(t)$.

where the sound field is given as a superposition of a continuum of plane waves. $\bar{S}(\alpha, \omega)$ denotes the spectral weight of the plane wave propagating in the direction of $\mathbf{n}_\alpha = (\cos\alpha, \sin\alpha, 0)$. The time-domain representation of (8) reads

$$s(\mathbf{x}, t) = \frac{1}{2\pi} \int_0^{2\pi} \bar{s}(\alpha, t) *_t \delta\left(t - \frac{r}{c}\cos(\phi-\alpha)\right) \mathrm{d}\alpha, \quad (9)$$

where $\bar{s}(\alpha, t)$ denotes the inverse Fourier transform of $\bar{S}(\alpha, \omega)$ and $*_t$ the time-domain convolution. For a spatially band-limited plane wave, the plane wave decomposition coefficients are merely weights given as a periodic sinc function [17, (4.95)] $\bar{S}(\alpha) = \bar{s}(\alpha) = \mathcal{D}_M(\alpha - \phi_{\mathrm{pw}})$ and the time-domain plane wave decomposition is given as

$$s(\mathbf{x}, t) = \frac{1}{2\pi} \int_0^{2\pi} \mathcal{D}_M(\alpha - \phi_{\mathrm{pw}}) \delta\left(t - \frac{r}{c}\cos(\phi-\alpha)\right) \mathrm{d}\alpha. \quad (10)$$

Since the argument of $\delta\left(t - \frac{r}{c}\cos(\phi - \alpha)\right)$ has only simple zeros for $t \in [-\frac{r}{c}, \frac{r}{c}]$ [18, (1.180a)]

$$\delta\left(t - \frac{r}{c}\cos(\phi-\alpha)\right) = \frac{\delta\left(\phi-\alpha-\beta(t)+\pi\right)+\delta\left(\phi-\alpha+\beta(t)+\pi\right)}{\frac{r}{c}|-\sin\beta(t)|},$$

with $-\frac{ct}{r} = \cos\beta(t)$. Equation (10) is thus rewritten as

$$s(\mathbf{x}, t) = \frac{1}{2\pi} \frac{\Pi(\frac{ct}{2r})}{\frac{r}{c}|\sin\beta(t)|} \quad (11)$$
$$\times \sum_{\mu\in\{\pm 1\}} \mu \int_\phi^{\phi+\mu\pi} \mathcal{D}_M(\alpha - \phi_{\mathrm{pw}}) \delta\left(\phi - \alpha + \pi + \mu\beta(t)\right) \mathrm{d}\alpha,$$

which leads to the same result as (5). Equation (11) shows more clearly that the sound field is a superposition of two plane waves. For brevity, the propagation angles are denoted as $\phi_{\mathrm{pw}}^{\pm}(t) \equiv \phi + \pi \pm \beta(t)$ with the corresponding normal vectors

$$\mathbf{n}_{\mathrm{pw}}^{\pm}(t) = (\cos\phi_{\mathrm{pw}}^{\pm}(t), \sin\phi_{\mathrm{pw}}^{\pm}(t), 0). \quad (12)$$

For $t = \pm\frac{r}{c}$, there is only one plane wave propagating in ϕ and $\phi + \pi$ respectively.

The spatial structure of a spatially band-limited plane wave is illustrated in Fig. 1. The wavefronts of two instantaneous plane waves intersect at $\mathbf{x}$. The circular wave front of radius $|ct|$ is a result of the superimposed plane waves, which converge toward the expansion center for $t < 0$ and then diverge for $t > 0$.

III. WAVE FIELD SYNTHESIS

The theory of WFS is based on the Kirchhoff-Helmholtz integral equation, which states that a homogeneous sound field within a source-free volume can be recreated by a continuous distribution of elementary sources on the surface. A high-frequency/far-field approximation is applied to the integral equation, thereby obtaining a formula that only consists of secondary monopoles. As a result, the driving function is given as the directional gradient of the desired sound field evaluated on the surface. For a more comprehensive introduction to WFS, the reader is referred to [3] and [5, Ch. 2].

In this paper, the desired sound field is synthesized by using a set of secondary point sources located in the xy-plane. Such a configuration is called 2.5-dimensional, due to the mismatch of the dimensionality between the sound field (2D) and the acoustic properties of the secondary sources (3D).

A. Driving Functions

The 2.5D WFS driving function for a plane wave with reference point $\mathbf{x}_{\text{ref}}$ reads [5, (2.177) and (2.178)]

$$D(\mathbf{x}_0, \mathbf{x}_{\text{ref}}, \omega) \tag{13}$$
$$= a(\mathbf{x}_0, \phi_{\text{pw}})\sqrt{i\frac{\omega}{c}}\sqrt{8\pi\|\mathbf{x}_0 - \mathbf{x}_{\text{ref}}\|}\langle\mathbf{n}_{\text{pw}}, \mathbf{n}_0(\mathbf{x}_0)\rangle e^{-i\frac{\omega}{c}\langle\mathbf{n}_{\text{pw}}, \mathbf{x}\rangle}$$

in the time-frequency domain and

$$d(\mathbf{x}_0, \mathbf{x}_{\text{ref}}, t) = h_{\text{eq}}(t) \tag{14}$$
$$*_t \left\{ a(\mathbf{x}_0, \phi_{\text{pw}})\sqrt{8\pi\|\mathbf{x}_0 - \mathbf{x}_{\text{ref}}\|}\langle\mathbf{n}_{\text{pw}}, \mathbf{n}_0(\mathbf{x}_0)\rangle\delta\big(t - \tfrac{\langle\mathbf{n}_{\text{pw}}, \mathbf{x}\rangle}{c}\big) \right\}$$

in the time domain. As illustrated in Fig. 2, the normal vector $\mathbf{n}_0(\mathbf{x}_0) = (\cos\phi_{\mathbf{n}}, \sin\phi_{\mathbf{n}}, 0)$ is an inward pointing vector defined for a given secondary source at $\mathbf{x}_0 \in \partial\Omega$. The secondary source selection window $a(\mathbf{x}_0)$ assures that the propagation of the synthesized sound field is correct [19, (5)]. For virtual plane waves, it is given as

$$a(\mathbf{x}_0, \phi_{\text{pw}}) = \begin{cases} 1, & \langle\mathbf{n}_{\text{pw}}, \mathbf{n}_0(\mathbf{x}_0)\rangle \geq 0 \\ 0, & \text{otherwise} \end{cases}. \tag{15}$$

The term $\sqrt{\|\mathbf{x}_0 - \mathbf{x}_{\text{ref}}\|}$ mediates the amplitude decay errors occurring in 2.5D WFS. In this paper, the expansion center is chosen as the reference point, $\mathbf{x}_{\text{ref}} = \mathbf{x}_c$.

The spectral weight $\sqrt{i\frac{\omega}{c}}$ in (13) is realized by the pre-equalization filter $h_{\text{eq}}(t)$ which is applied to the individual source signals or to the loudspeaker signals [19]. For convenience, $h_{\text{eq}}(t)$ is omitted in the following derivation.
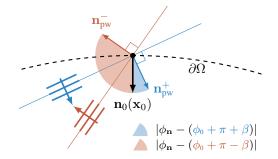

Fig. 2. Instantaneous plane waves passing a secondary source $\bullet \in \partial\Omega$. The plane waves ⇶ and ⇶ propagates in the direction of $\phi_0 + \pi + \beta(t)$ and $\phi_0 + \pi - \beta(t)$ respectively. The angles between the plane wave directions $\mathbf{n}_{\text{pw}}^{\pm}$ and the normal vector $\mathbf{n}_0$ are indicated by shaded arcs. According to the secondary source criteria (15), the blue plane wave is activated whereas the red plane wave is deactivated, since $\langle\mathbf{n}_{\text{pw}}^+, \mathbf{n}_0(\mathbf{x}_0)\rangle > 0$ and $\langle\mathbf{n}_{\text{pw}}^-, \mathbf{n}_0(\mathbf{x}_0)\rangle < 0$.

For the synthesis of a spatially band-limited plane wave, the driving function (14) is applied to the instantaneous plane waves in (7) and thus

$$d(\mathbf{x}_0, t) = \sqrt{\frac{2r}{\pi}}\frac{\Pi\big(\frac{ct}{2r}\big)}{\frac{r}{c}|\sin\beta(t)|} \tag{16}$$
$$\times \Big[a(\mathbf{x}_0, \phi_{\text{pw}}^+)\langle\mathbf{n}_{\text{pw}}^+(t), \mathbf{n}_0(\mathbf{x}_0)\rangle \mathcal{D}_M\big(\phi - \phi_{\text{pw}} + \pi + \beta(t)\big)$$
$$+ a(\mathbf{x}_0, \phi_{\text{pw}}^-)\langle\mathbf{n}_{\text{pw}}^-(t), \mathbf{n}_0(\mathbf{x}_0)\rangle \mathcal{D}_M\big(\phi - \phi_{\text{pw}} + \pi - \beta(t)\big) \Big].$$

Note the time-dependencies of the secondary source selection windows and the scalar products due to the varying plane wave directions.

An alternative time-domain driving function can be derived from plane wave decomposition (9)

$$d(\mathbf{x}_0, t) = \sqrt{\frac{2r}{\pi}}\int_0^{2\pi} a(\mathbf{x}_0, \alpha)\langle\mathbf{n}_\alpha, \mathbf{n}_0(\mathbf{x}_0)\rangle$$
$$\times \mathcal{D}_M(\alpha - \phi_{\text{pw}})\delta\big(t - \tfrac{r}{c}\cos(\phi - \alpha)\big)d\alpha, \tag{17}$$

where the plane wave driving function (14) is applied to the individual plane waves in (9).

IV. PRACTICAL IMPLEMENTATION

A. Discretization

To be implemented in a practical system, the driving function (16) has to be sampled uniformly in the time domain, i.e. $t_n = n/f_s$. Note that a sampling in the time domain constitutes a sampling of the plane wave directions $\phi_{\text{pw}}^{\pm}(t)$ for $|t| \leq \frac{r}{c}$. Due to the nonlinear dependency of $\phi_{\text{pw}}^{\pm}(t)$ on t, the sampled plane wave angles $\phi_{\text{pw}}^{\pm}(n/f_s)$ have a nonuniform distribution in $[0, 2\pi]$. For a given sampling frequency f_s, the number of plane waves is $N_{\text{pw}} \approx \frac{2r}{c}f_s$. For each secondary source, a different set of plane waves are selected.

A higher temporal resolution can be achieved by computing the driving function at a higher sampling rate, and then downsampling it to the original sampling rate. This will reduce the time-domain aliasing to some extent but not completely, since the Bessel functions in (1) are not band-limited [16, Ch. 9]. An analytic anti-aliasing filter can be used to suppress the aliasing artifacts, but this is out of the scope of this

paper. Using a higher sampling rate improves also the spatial resolution of the driving function, as the number of plane waves increases proportional to f_s.

The second driving function (17) is discretized separately in the temporal and spatial domain. In the time domain, the individual plane waves denoted by the Dirac delta function $\delta(\cdot)$ are realized by rounded integer delays or by fractional delay filters [20]. In either case, the signal carried by the plane wave is low-pass filtered thereby avoiding temporal aliasing. In the spatial domain, the plane wave angle α is discretized, and thus the integral is replaced by a summation. In this paper, uniform sampling is considered, $\alpha_\nu = \frac{2\pi\nu}{N_{pw}}$, $\nu = 0, \ldots, N_{pw} - 1$.

Although both sampling schemes are independent from each other, there is an interrelation when a large number of plane waves are synthesized in order to achieve a high spatial resolution. In this case, it is crucial to maintain a high temporal resolution by using fractional delay filters. Otherwise (using integer delays), two or more plane waves may have identical driving functions and increasing the number of plane waves has no benefit, similar to the observation in [21]. The number of required fractional delay filters is proportional to the number of plane waves and to the number of secondary sources. Therefore, higher spatial resolution comes at the cost of higher computational complexity.

B. Dynamic Range Control

If the driving function is sampled close to $t = \pm\frac{r}{c}$, the term $\frac{1}{|\sin\beta(t)|}$ in (16) tends to infinity. To avoid numerical problems, a soft-knee limiting function,

$$\mathcal{L}(u) = \frac{2A_{thr}}{\pi} \arctan\left(\frac{\pi u}{2A_{thr}}\right), \qquad (18)$$

is applied to the latter term, where the threshold A_{thr} determines its maximum value. Note that the driving function is more compressed around $t = \pm\frac{r}{c}$ where most of the high-frequency components are present. Such a dynamic range control thus has a low-pass filtering effect and alleviates the effects of temporal aliasing.

V. EVALUATION

The driving functions proposed in this paper are used for the synthesis of a virtual plane wave. The plane wave is assumed to propagate parallel to the xy-plane with an azimuth angle $\phi_{pw} = -\frac{\pi}{2}$. The desired sound field is expanded with respect to an expansion center up to the order of $M = 29$. A circular array of 60 secondary sources are used which are equiangularly placed on a circle with radius of 1.5 m. The secondary sources are assumed to be ideal point sources. The sampling frequency is set to $f_s = 44.1$ kHz and the speed of sound is assumed to be $c = 343$ m/s.

The time-domain driving function (16) is shown in Fig. 3 (top) for different expansion positions, $\mathbf{x}_c = (0,0,0)$ and $(0.5,0,0)$. The peaks of the driving functions are found on the same v-shaped contour, but the detailed temporal structure differs due to the spatial shift of the harmonics expansion. The acausality of the driving functions is attributed to the definition
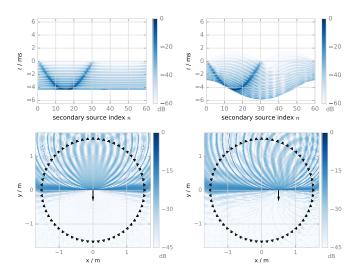

Fig. 3. Driving functions (top row) computed according to (16) and the synthesized sound fields (bottom row) of a spatially band-limited plane wave ($M = 29$, $\phi_{pw} = -\frac{\pi}{2}$). The expansion center is $\mathbf{x}_c = (0,0,0)$ in the left column and $\mathbf{x}_c = (0.5,0,0)$ in the right column. The snapshots of the sound fields are taken at $t = 0$ ms. The plane wave directions are indicated by black arrows, the base of which lies on the respective expansion center. The secondary sources ($N = 60$) are uniformly distributed on a circle ($r_0 = 1.5$ m).

of the plane wave which passes the origin at $t = 0$. For a practical implementation, a pre-delay has to be applied.

The driving functions are used for the synthesis of the desired sound field, and the time snapshots ($t = 0$ ms) of the synthesized sound fields are shown in Fig. 3 (bottom). The direction of the desired plane wave is indicated by black arrows, and the base of each arrow is placed on the center of expansion $\mathbf{x}_c$. The narrow wavefront observed around $\mathbf{x}_c$ indicates that the local sound field exhibits a high accuracy throughout a wide frequency range. In lateral positions, on the other hand, a low-pass filtered response is expected because of the wide wavefront. This agrees with the observation in the previous study [13]. Note also that the sound field for $\mathbf{x}_c = (0,0,0)$ resembles the sound field of a typical NFC-HOA system [7, Fig. 5.16] where a similar spatial band-limitation was applied.

The spectral properties of the synthesized sound fields are examined in Fig. 4. The results in the bottom row are computed with an oversampled rate $f_s^\uparrow = 2 \times f_s = 88.2$ kHz. The leftmost column shows the influence of the dynamic range control introduced in IV-B. The higher the threshold, the more high frequency components are observed. Nearly flat responses were obtained with $A_{thr} = 17$ (top) and $A_{thr} = 24$ (bottom).

The right six figures in Fig. 4 show the frequency responses of the synthesized sound field at different receiver positions which coincide with the respective expansion center $\mathbf{x}_c$. Here, the proposed driving function (CHT) is compared with the driving function given in (17). The latter was implemented with and without fractional delay filters (PWD-f and PWD-i, respectively). For PWD-f, 20-th order Lagrange filters were used. As can be seen, the proposed driving function (CHT) achieves a comparable performance to the implementation
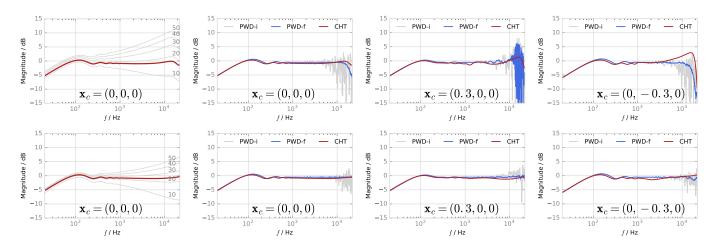
Fig. 4. Frequency responses of the synthesized sound field. The driving function (16) is computed with (bottom, $f_s^\uparrow = 88.2$ kHz) and without (top, $f_s = 44.1$ kHz) oversampling. The corresponding number of plane waves are 385 and 771, respectively. The influence of dynamic range control is shown in the leftmost column where A_{thr} is varied between 10 and 50 with interval of 10. $A_{thr} = 17$ (top) and $A_{thr} = 24$ (bottom) achieve nearly flat responses (red lines). The right three columns compare the driving functions (16) (CHT) and (17) (PWD-i: integer delay, PWD-f: fractional delay).

using fractional delay filters, with a much lower computational cost.

Oversampling the driving function clearly improves the spectral accuracy. It removes the high frequency bump which is a result of temporal aliasing. The low frequency roll-off is a typical characteristic of WFS, which is attributed to the high-frequency approximations mentioned in III.

VI. CONCLUSION

In this paper, a time-domain WFS driving function is introduced for the synthesis of a spatially band-limited plane wave. It is based on the analytic time-domain representation of the sound field, which was derived directly from the circular harmonics expansion as well as from the plane wave decomposition. It was shown that the time-domain sound field can be interpreted as a continuum of plane waves, and the amplitudes and directions of the instantaneous plane waves were identified. Based on the analytic representation, the WFS driving function was derived and used in a 2.5D scenario. The proposed driving function is able to synthesize a plane wave with an improved local accuracy, which suggests its usage for local sound field synthesis. The spectral distortion of the sound field is comparable to the direct implementation of plane wave decomposition, but with a much lower computational complexity.

It is still an open question how to perform the dynamic range control and anti-aliasing filtering at the same time. Although an optimal value for A_{thr} can be found empirically, a more sophisticated method is desirable. Perceptual evaluation and comparison with other existing local WFS approaches [22], [23] remain as future work.

REFERENCES

[1] A. J. Berkhout, D. de Vries, and P. Vogel, "Acoustic Control by Wave Field Synthesis," *J. Acoust. Soc. Am. (JASA)*, vol. 93, no. 5, pp. 2764–2778, 1993.
[2] J. Daniel, "Spatial Sound Encoding including Near Field Effect: Introducing Distance Coding Filters and a Viable, new Ambisonic Format," in *Proc. 23rd Audio Eng. Soc. (AES) Int. Conf.*, Helsingør, Denmark, 2003.
[3] S. Spors, R. Rabenstein, and J. Ahrens, "The Theory of Wave Field Synthesis Revisited," in *Proc. 124th Audio Eng. Soc. (AES) Conv.*, 2008.
[4] J. Ahrens and S. Spors, "An Analytical Approach to Sound Field Reproduction using Circular and Spherical Loudspeaker Distributions," *Acta Acust. united with Ac.*, vol. 94, no. 6, pp. 988–999, 2008.
[5] F. Schultz, "Sound Field Synthesis for Line Source Array Applications in Large-Scale Sound Reinforcement," Ph.D. dissertation, University of Rostock, 2016.
[6] B. Girod, A. Stenger, and R. Rabenstein, *Signals and systems*. Wiley, 2001.
[7] J. Ahrens, *Analytic Methods of Sound Field Synthesis*. Springer, 2012.
[8] J. Ahrens and S. Spors, "Alterations of the Temporal Spectrum in High-Resolution Sound Field Reproduction of Different Spatial Bandwidths," in *Proc. 126th Audio Eng. Soc. (AES) Conv.*, Munich, Germany, May 2009.
[9] S. Spors and J. Ahrens, "A Comparison of Wave Field Synthesis and Higher-order Ambisonics with respect to Physical Properties and Spatial Sampling," in *Proc. 125th Audio Eng. Soc. (AES) Conv.*, San Fransisco, USA, Oct. 2008.
[10] H. Wierstorf, A. Raake, and S. Spors, "Localization in Wave Field Synthesis and Higher Order Ambisonics at different positions within the listening area," in *Proc. 39th German Annu. Conf. on Acoust. (DAGA)*, Meran, Italy, Mar. 2013.
[11] J. Ahrens and S. Spors, "An Analytical Approach to Sound Field Reproduction with a Movable Sweet Spot Using Circular Distributions of Loudspeakers," in *Proc. Int. Conf. Acoust. Speech Signal Process. (ICASSP)*, Taipei, Taiwan, Apr. 2009.
[12] F. Winter, J. Ahrens, and S. Spors, "On Analytic Methods for 2.5-D Local Sound Field Synthesis Using Circular Distributions of Secondary Sources," *IEEE/ACM Trans. Audio, Speech, and Language Process.*, vol. 24, no. 5, pp. 914–926, 2016.
[13] N. Hahn, F. Winter, and S. Spors, "Local Wave Field Synthesis by Spatial Band-limitation in the Circular/Spherical Harmonics Domain," in *Proc. 140th Audio Eng. Soc. (AES) Conv.*, Paris, France, Jun. 2016.
[14] H. Teutsch, *Modal Array Signal Processing: Principles and Applications of Acoustic Wavefield Decomposition*. Springer, 2007, vol. 348.
[15] R. A. Kennedy, P. Sadeghi, T. D. Abhayapala, and H. M. Jones, "Intrinsic Limits of Dimensionality and Richness in Random Multipath Fields," *IEEE Trans. Signal Process.*, vol. 55, no. 6, pp. 2542–2556, 2007.
[16] M. Abramowitz and I. A. Stegun, *Handbook of Mathematical Functions: with Formulas, Graphs, and Mathematical Tables*. Courier Corporation, 1964, no. 55.
[17] A. Kuntz, *Wave Field Analysis using Virtual Circular Microphone Arrays*. Verlag Dr. Hut, 2008.
[18] G. B. Arfken and H. J. Weber, *Mathematical Methods for Physicists*. Harcourt/Academic Press, 2001.
[19] S. Spors, "Extension of an Analytic Secondary Source Selection Criterion for Wave Field Synthesis," in *Proc. 123rd Audio Eng. Soc. (AES) Conv.*, New York, USA, Oct. 2007.
[20] T. I. Laakso, V. Valimaki, M. Karjalainen, and U. K. Laine, "Splitting the Unit Delay," *IEEE Signal Process. Mag.*, vol. 13, no. 1, pp. 30–60, 1996.
[21] F. Winter and S. Spors, "On Fractional Delay Interpolation for Local Wave Field Synthesis," in *Proc. Eur. Signal Process. Conf. (EUSIPCO)*, Budapest, Hungary, Aug. 2016.
[22] S. Spors and J. Ahrens, "Local Sound Field Synthesis by Virtual Secondary Sources," in *Proc. 40th Audio Eng. Soc. (AES) Int. Conf. Spatial Audio*, Tokyo, Japan, Oct. 2010.
[23] S. Spors, K. Helwani, and J. Ahrens, "Local Sound Field Synthesis by Virtual Acoustic Scattering and Time-reversal," in *Proc. 131th Audio Eng. Soc. (AES) Conv.*, New York, USA, Oct. 2011.